Observations of high-energy electron distributions in laser plasmas

R. L. Keck, L. M. Goldman, M. C. Richardson, W. Seka, and K. Tanaka
Laboratory for Laser Energetics, University of Rochester, 250 East River Road, Rochester, New York 14623

(Received 19 March 1984; accepted 5 July 1984)

A very energetic (20–60 keV) electron distribution is observed in laser plasmas produced with both 1054 and 351 nm drivers. This component, believed to be generated by the $2\omega_p$ instability, is present at intensities above approximately 2×10^{14} W/cm^2 and contains less than 0.1% of the incident energy. For 1054 nm irradiation, this component appears in addition to the 2 to 7 keV distribution attributed to resonance absorption.

I. INTRODUCTION

A major reason for the interest in short-wavelength ($\lambda\leqslant500$ nm) high-intensity lasers for use as laser fusion drivers is that absorption occurs primarily through inverse bremsstrahlung rather than resonance absorption, thus avoiding the generation of suprathermal electrons. However, parametric instabilities occurring in the underdense plasma may also produce fast electrons,[1,2] and the signatures of these instabilities have been observed with various wavelength drivers.[3–6] Fast electrons produced by these instabilities have been observed in underdense plasmas in interactions with longer-wavelength lasers.[7–9]

In this paper, we report observations of high-energy electron distributions, produced in dense plasmas by 1054 and 351 nm drivers, which were measured indirectly by observing the bremsstrahlung x-ray continuum spectrum. This high-energy component, which we attribute to the presence of the two plasmon decay ($2\omega_p$) instability, is present above a threshold intensity of approximately 2×10^{14} W/cm^2 and appears to saturate above about 4×10^{14} W/cm^2. For 1054 nm incident radiation it appears in addition to the component produced by resonance absorption. No evidence of resonance absorption is observed with 351 nm irradiation.

II. EXPERIMENT

The 1054 nm experiments were conducted on the 24 beam OMEGA laser system.[10] The laser beams were focused tangentially, eight target radii behind target center, so that each beam illuminated a target hemisphere. The resulting overlap of the beams helps to ensure highly uniform target illumination with an rms nonuniformity of less that 6%.[11] The targets used were solid plastic (CH) spheres. The intensity was varied between approximately 5×10^{13} and 2×10^{15} W/cm^2 by using 200, 400, and 600 μm diameter targets, and by varying the laser energy. The laser pulse duration was approximately 0.9 nsec.

The 351 nm experiments were performed on the single beam frequency-tripled GDL laser system.[12] Targets were planar plastic (CH) and effectively of infinite mass. The intensity on target was varied by changing both laser energy and focal position with the focal spot diameter ranging from 100 to 300 μm. Both 0.5 and 0.9 nsec laser pulse lengths were used. In order to assess the importance of geometric effects, a small number of shots were made at 1054 nm on the GDL system.

The x-ray continuum was measured using K-edge filtered detectors consisting of an array of nine silicon PIN diodes and six NaI scintillators coupled to photomultiplier tubes (PMT's). The detector arrays incorporated lead shields and collimators to minimize pickup of x rays from the target chamber walls. The PMT detectors were calibrated using Am^{241} and Co^{60} nuclear sources; the sensitivity of the PIN diodes was calculated on the basis of the manufacturers thickness specifications and the band gap energy of silicon which is well known. The charge pulses from the detectors were integrated and recorded using gated analog to digital converters. Additional oscilloscope monitoring was utilized to check for noisy or saturated signals. Table I shows the detectors and filtering used.

The response function for a typical K-edge filtered detector is shown in Fig. 1. While the peak response occurs in a narrow band just below the K-edge energy of the filter, there is also a broad low-level sensitivity at energies above the K-edge. For a low-temperature plasma, the spectral intensity, $dE/dh\nu$, will decrease with $h\nu$ rapidly enough that the spectrally weighted detector response is effectively a narrow band as shown. In this case, the signal from the detector is proportional to $dE/dh\nu$ at the midband value of $h\nu$, and a local measurement of the spectrum is obtained. In these experiments, the measured spectra indicate a temperature sufficiently high that the detector responses are not generally narrow band. This requires that the spectrum be obtained globally rather than just locally.

TABLE I. K-edge detector system configuration.

Filter material	Filter thickness	K-edge (keV)	Detector material	Detector thickness	Detector type
Cl (Saran)	50 μm	2.8	Si	250 μm	PIN
Sc	28	4.5	Si	250	PIN
Fe	25	7.1	Si	250	PIN
Ni	20	8.3	Si	250	PIN
Zn	47	9.7	Si	250	PIN
Y	253	17.0	Si	250	PIN
Mo	113	20.0	Si	250	PIN
As	136	25.5	Si	250	PIN
As	254	25.5	NaI	1 mm	PMT
Sn	250	29.2	NaI	1	PMT
Ta	507	67.4	NaI	1	PMT
Pb	1.0 mm	88.0	NaI	1	PMT
Pb	2.5	88.0	NaI	50	PMT
Pb	5.7	88.0	NaI	50	PMT

 0031-9171/84/112762-05$01.90 © 1984 American Institute of Physics

Downloaded 31 Oct 2003 to 132.170.162.242. Redistribution subject to AIP license or copyright, see http://ojps.aip.org/phf/phfcr.jsp

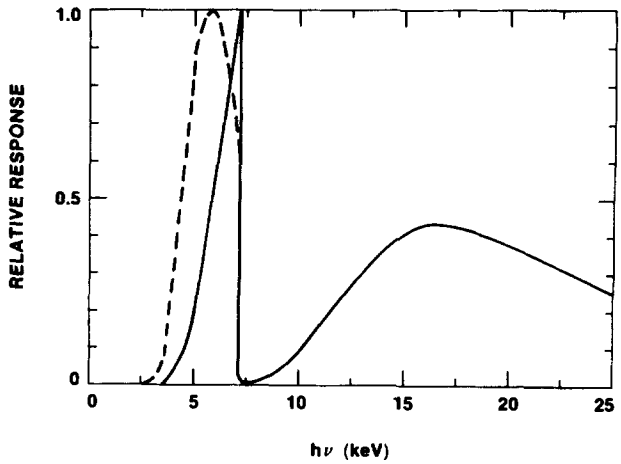

FIG. 1. Response function of a typical K-edge detector. The effective response obtained with a 1 keV temperature spectrum is also shown.

Several approaches for obtaining a global fit exist. One straightforward approach is to use a multigroup method and divide the spectrum into a set of energy bins. A disadvantage of this approach is that the partitioning of the spectrum is completely arbitrary, and a different fit will be obtained for each choice of energy partitioning. In order to avoid this problem, and to minimize the number of parameters required to describe the spectrum, we use a multi-Maxwellian model for the spectrum. This is done by assuming that the spectrum can be approximated by

$$\frac{dE}{dh\nu} = \sum_{j=1}^{K} N_j \exp\left(\frac{-h\nu}{T_j}\right), \tag{1}$$

where N_j and T_j are parameters determined through a least square fit to the measured data. If the electron distribution actually consists of K Maxwellian components, then the parameter T_j represents the temperature of the corresponding jth Maxwellian. Since the measurement is both time and space integrated and the actual electron distribution is not known, the value of T_j should only be loosely interpreted as representing an actual electron temperature. The multi-Maxwellian model may appear to be overly restrictive. However, previous experimental work shows the electron spectrum to be exponential in character, particularly for the case of resonanance absorption.[13,14] Also, numerical simulations of resonance absorption[15] and the Raman[16] and $2\omega_p$ instabilities[1] predict electron distributions which are approximately Maxwellian. Finally, we find that for a suitable choice of K, good fits to the data are obtained.

The energy E_j in a nonthermal electron distribution may be obtained from the parameter N_j as

$$E_j = N_j/(1.6\times 10^{10}\langle Z^2\rangle/\langle Z\rangle) \text{ (joules)}. \tag{2}$$

This expression, derived by Brueckner,[17] assumes that fast electrons lose their energy primarily through collisions with a cold background plasma, and neglects losses to fast ions or processes which could enhance the radiation rate. It depends only weakly on plasma conditions through the Coulomb logarithm ($\ln\Lambda$) and is relatively insensitive to the actual electron distribution. In Eq. (2), we use $\ln\Lambda = 4.5$, corresponding to the electron energy loss occurring in dense material. Brueckner evaluated $\ln\Lambda$ at an electron density of 10^{21} cm^{-3}, obtaining a value a factor of 2 higher [Eq. (18) of Ref. 17 with $I_n(0)\ln\Lambda = 2$].

III. RESULTS

The x-ray continuum spectra obtained using 351 nm irradiation in planar geometry on GDL are distinctly different from those obtained using 1054 nm irradiation whether in planar geometry on GDL or spherical geometry on OMEGA. At intensities above 2×10^{14} W/cm^2 the spectra from 351 nm experiments can be well fit using the least squares procedure previously described with only two Maxwellian components, while the spectra from 1054 nm experiments require three Maxwellian components to adequately fit the data. The determination of the number of Maxwellians required to fit a particular set of data is made by inspection of the residuals as well as the normalized χ^2. For example, χ^2 typically improves by more than a factor of 5 when a three-Maxwellian model is used to fit the 1054 nm data rather than a two-Maxwellian model. Also, attempts to fit 1054 nm data with a two Maxwellian model usually result in bistable convergence of the fitting routine, where either one of two equally good solutions can be obtained depending on the initial temperature estimates.

We shall refer to the three components observed at 1054 nm as cold, hot, and superhot. A hot component is not observed with 351 nm irradiation. The temperature and intensity dependence of each component provides a means of determining the origin of the underlying electron temperature distribution. The cold component, which is always observed with either 351 or 1054 nm irradiation, has a temperature of 600–800 eV. Clearly it is produced by electrons in the high-density thermal plasma near n_c. There is no observable scaling of the cold temperature with intensity over the range of intensities used in these experiments. The temperature and intensity dependence of the hot component, which will be discussed in detail in a subsequent section, indicate that it is produced by electrons generated by resonance absorption. The superhot component can, on the basis of its intensity dependence and the intensity dependence of harmonic light emission measurements, be attributed to the production of very fast electrons by parametric instabilities occurring near $n_c/4$. This component is observed with either 351 or 1054 nm irradiation. In the following section the superhot component will be considered in detail.

A. The superhot spectral component

The temperature of the superhot component measured on the 1054 nm OMEGA experiments is shown in Fig. 2. Since the superhot component is attributed to quarter-critical parametric instabilities, the intensity scale has been corrected for the excursion of the quarter-critical surface, $n_c/4$. On the basis of spatially resolved measurements of 3/2 harmonic emission from the target[18] and numerical results obtained with the hydrodynamic codes SAGE and LILAC, $n_c/4$ is located approximately 120 μm from the initial target surface at the peak of the laser pulse. When this correction is made, the data spans such a limited intensity range and its

Downloaded 31 Oct 2003 to 132.170.162.242. Redistribution subject to AIP license or copyright, see http://ojps.aip.org/phf/phfcr.jsp

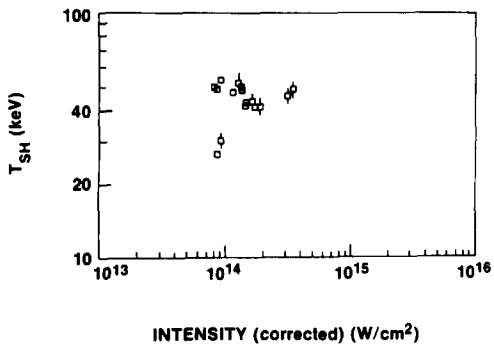

FIG. 2. Superhot x-ray temperature as a function of nominal incident intensity at 1054 nm with 24 beam spherical geometry. The intensity is that incident at $n_c/4$ and has been corrected to account for the excursion of $n_c/4$ at the peak of the laser pulse.

scatter is so high that it is impossible to draw any conclusions on the temperature scaling with intensity.

In contrast, the 0.5 nsec, 351 nm data obtained on the GDL experiments (Fig. 3) does indicate a slow $I^{0.2}$ scaling with intensity. It should be noted that the intensity on GDL is not well defined since the beam is not uniform. The intensity plotted here for the GDL data is 1.5 times the average intensity, where the factor 1.5 is intended to weight the peak intensities more heavily, since the parametric instabilities of interest here will be driven by the highest-intensity portions of the beam. This same intensity nonuniformity may distort the measured scaling of quantities which have a threshold behavior if they are measured near threshold. Taking beam nonuniformity into account, we estimate, by integrating an I^n-type intensity scaling with an intensity threshold over an intensity distribution similar to that of the GDL beam, that the measured $I^{0.2}$ temperature scaling may correspond to an actual $I^{0.3}$ scaling of T_{sh} with intensity. This would be in reasonable agreement with the $(I\lambda^2)^{1/3}$ scaling of the electron temperature produced by quarter-critical parametric instabilities predicted in Ref. 19. The $(I\lambda^2)^{1/3}$ law also indicates that there should be a scaling of T_{sh} as $\lambda^{2/3}$. Because of the previously mentioned problems with the T_{sh} measurement at 1054 nm, it can only be noted that T_{sh} does decrease with wavelength by a factor of about the right order.

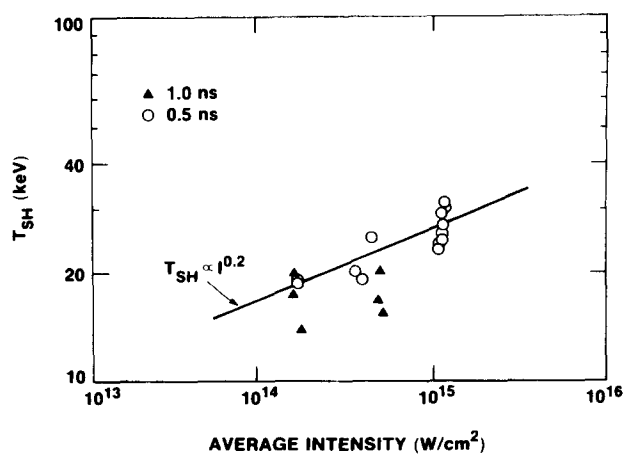

FIG. 3. Superhot x-ray temperature as a function of incident intensity at 351 nm with single beam planar geometry.

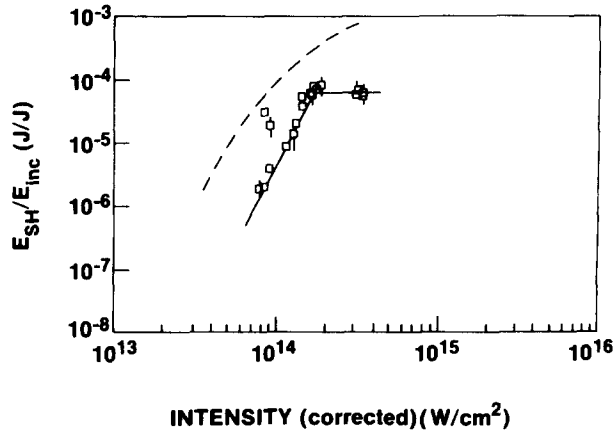

FIG. 4. Fraction of incident energy contained in the superhot electron distribution at 1054 nm as inferred from the x-ray intensity (solid curve). Also shown is the relative $3\omega_0/2$ harmonic signal (dashed curve).

The relative energy in the superhot electron component measured on 1054 nm experiments on OMEGA, as determined from N_H using Brueckner's model, is shown in Fig. 4. A clear threshold behavior is seen with E_{sh}/E_{inc} decreasing rapidly below about 2×10^{14} W/cm^2 and saturating above this intensity. The dashed curve in Fig. 4 shows the relative energy in the $3/2\omega_0$ signal from the target. This is a signature of plasma wave producing instabilities, e.g., Raman and $2\omega_p$, at $n_c/4$. A reasonably strong correlation between the $3/2\omega_0$ signal and electron energy can be observed.

The relative energy in the superhot component measured in the 351 nm GDL experiments is shown in Fig. 5. Again a rise and saturation behavior is evident. Also plotted is the $\omega_0/2$ signal produced by $2\omega_p$ (Ref. 3). Again the x-ray signal and $\omega_0/2$ signal track remarkably closely. Figure 6 shows the scaling of E_{sh}/E_{inc} obtained from an early, more extensive data set at 351 nm on GDL. Because of less than optimal filtering, the absolute magnitude of the data is less well determined than the data presented in Fig. 5. However, it better illustrates the detailed scaling of E_{sh}/E_{inc} with intensity. Also shown in Fig. 6 is the relative signal from the Raman instability (curve a) and the $2\omega_p$ instability (curve b) obtained in Ref. 3. Production of $\omega_0/2$ by the Raman insta-

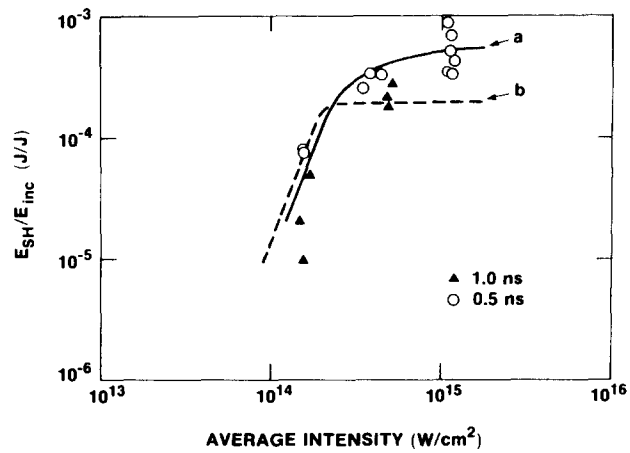

FIG. 5 Fraction of incident energy contained in the superhot electron distribution at 351 nm as inferred from the x-ray intensity (curve a). Also shown is the relative $3\omega_0/2$ harmonic signal (from Ref. 3) (curve b).

Downloaded 31 Oct 2003 to 132.170.162.242. Redistribution subject to AIP license or copyright, see http://ojps.aip.org/phf/phfcr.jsp

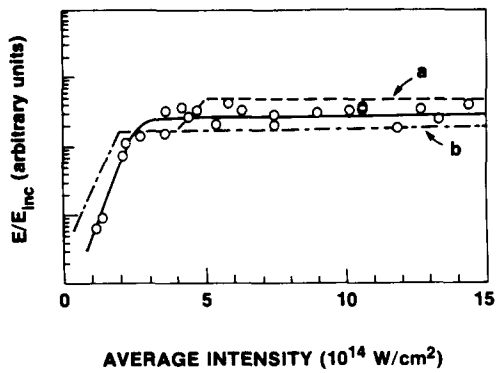

FIG. 6. Fraction of incident energy contained in the superhot electron distribution from an early data set at 351 nm on GDL (solid curve). The absolute magnitude of the data is not as well determined as that of the data shown in Fig. 5, but these data better show the scaling with intensity. The $\omega_0/2$ harmonic signal (from Ref. 3) is also shown where curve b is the component produced by the $2\omega_p$ instability and curve a is the component produced by the Raman instability.

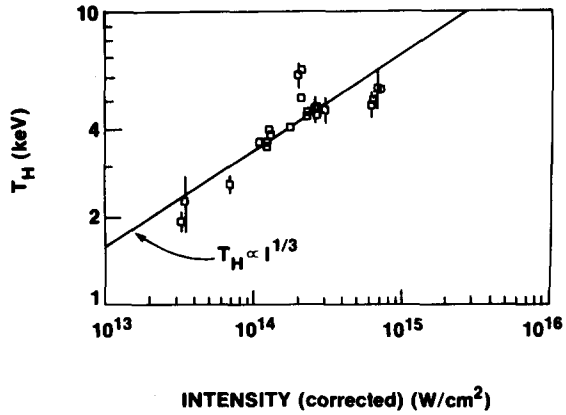

FIG. 7. Hot x-ray temperature as a function of nominal intensity at 1054 nm. The solid curve has a slope of 1/3.

bility is direct, while for the $2\omega_p$ instability it is indirect and hence much less efficient. So while in Fig. 6, $\omega_0/2$ production by the Raman instability somewhat exceeds that by the $2\omega_p$ instability, the $2\omega_p$ instability is more important and we conclude that the superhot electron component is being produced primarily by the $2\omega_p$ instability. The fact that there is no observable increase in x-ray production when the Raman instability starts to occur confirms this.

Comparison of Figs. 4 and 5 shows that the saturated value of E_{sh}/E_{inc} is considerably larger at 351 nm than at 1054 nm. Because the absorption is also higher at 351 nm than at 1054 nm, the saturated value of E_{sh}/E_{abs} is only about a factor of two larger at 351 nm than at 1054 nm.

B. The hot spectral component

Although the superhot electron component was of primary interest in these experiments, in the case of 1054 nm irradiation the expected hot component from resonance absorption was also observed. The temperature of the hot component measured in the OMEGA 1054 nm experiments is plotted as a function of incident intensity in Fig. 7. In this case the intensity is corrected for the excursion of n_c. On the basis of second-harmonic emission measurements and code calculations n_c is located approximately 55 μm from the initial target surface. An approximate $I^{1/3}$ scaling is observed throughout the measured intensity range. The intensity-corrected data are in reasonable agreement with previous experimental work[14,20] and scaling obtained from numerical simulation of resonance absorption,[15] with the temperatures measured here being somewhat lower than found in Ref. 14.

The energy in the hot electron component relative to energy absorbed is shown in Fig. 8 along with the measured absorption of the incident laser. The energy in the hot electron component is somewhat higher than expected. For example, Ref. 14 measures $E_H/E_{abs} \approx 0.30$ at 10^{15} W/cm^2 [note that we have obtained this value indirectly from Ref. 14 by applying Brueckner's model to data presented in Figs. 1(b) and 2(a) of Ref. 14]. Calculations by the hydrodynamic code LILAC show approximately 14% of the absorbed energy in fast electrons[21] at 10^{15} W/cm^2 (this is exclusive of the energy which is transferred to fast ions, which is not detected in our measurements). Thus, it appears that the measured values of E_H/E_{abs} may be a factor of 2 to 4 high. However, the error bars on the measured E_H/E_{abs} indicate an uncertainty of nearly a factor of 2, most of which is systematic. In addition, because the measured T_H is comparable to the coronal temperature, a possible source of bias is unresolved contributions to the spectrum from the coronal plasma. This contribution would tend to decrease the measured T_H while increasing the measured E_H/E_{abs}. Thus, while we do not believe that E_H can be determined with sufficient accuracy at these low values of T_H to make these measurements particularly useful for determining the resonance absorption fraction in these experiments, they do indicate that our measurements are basically sound. Since the superhot component is hot enough to be unaffected by lower-temperature components, the determination of E_{sh} should certainly be better than a factor of 4 and is probably within the error limits shown in the figures.

IV. CONCLUSIONS

The x-ray continuum spectra from plasmas produced with 1054 and 351 nm irradiation have been measured. From these we have obtained the temperatures and relative

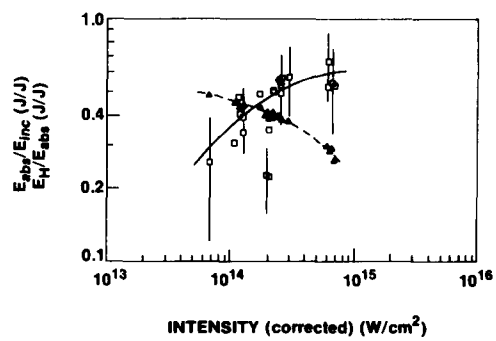

FIG. 8. Fraction of absorbed energy contained in the hot electron distribution at 1054 nm as inferred from the x-ray intensity (square symbols, solid curve). Also shown is the measured absorption (triangular symbols, dashed curve).

Downloaded 31 Oct 2003 to 132.170.162.242. Redistribution subject to AIP license or copyright, see http://ojps.aip.org/phf/phfcr.jsp

energies of suprathermal electron distributions present in the plasmas. We find that:

(a) There is a superhot electron distribution present in both 351 and 1054 nm produced plasmas which saturates at less than 10^{-3} of the absorbed energy at intensities above 6×10^{14} W/cm^2.

(b) On the basis of the correlation of the intensity scaling of the superhot energy and harmonic light emission from the target, the superhot distribution may be attributed the presence of the $2\omega_p$ instability.

(c) The lack of an observable hot electron component at 351 nm, as well as the high measured absorptions and low preheat at 351 nm,[22,23] confirm that the absorption of 351 m laser light is dominated by inverse bremsstrahlung. While the level of superhot electron production measured here would not be serious for laser fusion, the targets and scale lengths in these experiments were too small to allow this result to be generalized to reactor-sized targets. Fast electron production by underdense plasma instabilities will need to be monitored in future experiments which utilize larger targets with longer scale lengths.

ACKNOWLEDGMENTS

The authors would like to acknowledge valuable discussions with Dr. R. S. Craxton, Dr. J. Delettrez, and Dr. B. Yaakobi.

This work was partially supported by the U. S. Department of Energy Inertial Fusion Project under Contract No. De-AC08-80DP40124 and by the Laser Fusion Feasibility Project at the Laboratory for Laser Energetics which has the following sponsors: General Electric Company, Northeast Utilities, New York State Energy Research and Development Authority, The Standard Oil Company (Ohio), The University of Rochester, and Empire State Electric Energy Research Corporation. Such support does not imply endorsement of the content by any of the above parties.

[1]A. B. Langdon, B. F. Lasinski, and W. L. Kruer, Phys. Rev. Lett. **43,** 133 (1979).

[2]K. Estabrook, W. L. Kruer, and B. F. Lasinski, Phys. Rev. Lett **45,** 1399 (1980).

[3]K. Tanaka, L. M. Goldman, W. Seka, M. C. Richardson, J. M. Soures, and E. A. Williams, Phys. Rev. Lett. **48,** 1179 (1982).

[4]K. Tanaka and L. M. Goldman, Phys. Rev. Lett. **45,** 1558 (1980).

[5]D. W. Phillion, D. L. Banner, E. M. Campbell, R. E. Turner, and K. G. Estabrook, Phys. Fluids **25,** 1434 (1982).

[6]D. M. Villeneuve, R. L. Keck, B. B. Afeyan, W. Seka, and E. A. Williams, Phys. Fluids **27,** 721 (1984).

[7]D. W. Phillion, E. M. Campbell, K. G. Estabrook, G. E. Phillips, and F. Ze, Phys. Rev. Lett. **49,** 1405 (1982).

[8]R. G. Berger, R. D. Brooks, and Z. A. Pietrzyk, Phys. Fluids **26,** 354 (1983).

[9]N. A. Ebrahim, H. A. Baldis, C. Joshi, and R. Benesch, Phys. Rev. Lett. **45,** 1179 (1980).

[10]J. Bunkenberg, J. Boles, D. C. Brown, J. Eastman, J. Hoose, R. Hopkins, L. Iwan, S. D. Jacobs, J. H. Kelly, S. Kumpan, S. Letzring, D. Lonobile, L. D. Lund, G. Mourou, S. Refermat, W. Seka, J. M. Soures, and K. Walsh, IEEE J. Quantum Electron. **QE-17,** 1620 (1981).

[11]M. C. Richardson, T. R. Boehly, B. A. Brinker, T. C. Bristow, R. S. Craxton, J. A. Delettrez, G. Enright, A. Entenberg, W. Friedman, L. M. Goldman, J. Hoose, R. J. Hutchinson, L. Iwan, S. Kacenjar, K. Lee, S. A. Letzring, L. D. Lund, R. S. Marjoribanks, R. L. McCrory, J. M. Miller, J. Rizzo, W. Seka, S. Skupsky, J. M. Soures, C. P. Verdon, D. M. Villeneuve, E. A. Williams, and B. Yaakobi, in *Laser Interaction and Related Plasma Phenomena*, edited by H. Hora and H. Miley (Plenum, New York, 1984), Vol. 6.

[12]W. Seka, J. M. Soures, S. D. Jacobs, L. D. Lund, and R. S. Craxton, IEEE J. Quantum Electron. **QE-17,** 1689 (1981).

[13]C. M. Armstrong, B. H. Ripin, F. C. Young, R. Decoste, R. R. Whitlock, and S. E. Bodner, J. Appl. Phys. **50,** 5233 (1979); W. Priedhorsky, D. Lier, R. Day, and D. Gerke, Phys. Rev. Lett. **47,** 1661 (1981).

[14]D. C. Slater, Gar. E. Busch, G. Charatis, R. R. Johnson, F. J. Mayer, R. J. Schroeder, J. D. Simpson, D. Sullivan, J. A. Tarvin, and C. E. Thomas, Phys. Rev. Lett. **46,** 1199 (1981).

[15]K. Estabrook and W. L. Kruer, Phys. Rev. Lett. **40,** 42 (1978).

[16]K. Estabrook, W. L. Kruer, and B. F. Lasinski, Phys. Rev. Lett. **45,** 1399 (1980).

[17]K. A. Brueckner, Nucl. Fusion **17,** 1257 (1977).

[18]M. C. Richardson, S. Skupsky, J. Kelly, L. Iwan, R. Hutchinson, R. Peck, R. L. McCrory, and J. M. Soures, in *Proceedings of the 1983 Los Alamos Conference on Optics*, edited by R. S. McDowell and S. C. Stotlar (S.P.I.E., Bellingham, WA, 1983), Vol. 380.

[19]B. F. Lasinski, A. B. Langdon, K. G. Estabrook, and W. L. Kruer, Lawrence Livermore 1980 Annual Report No. UCRL-50021-80, 1981, pp. 3–30.

[20]K. R. Manes, H. G. Ahlstrom, R. A. Haas, and J. F. Holzrichter, J. Opt. Soc. Am. **67,** 717 (1977).

[21]B. Yaakobi, J. Delettrez, L. M. Goldman, R. L. McCrory, R. Marjoribanks, M. C. Ricardson, D. Shvarts, S. Skupsky, J. M. Soures, C. Verdon, D. M. Villeneuve, T. Boehly, R. Hutchinson, and S. Letzring, Phys. Fluids **27,** 516 (1984).

[22]W. Seka, R. S. Craxton, J. Delettrez, R. Keck, R. L. McCrory, D. Shvarts, J. M. Soures, and R. Boni, Opt. Commun. **40,** 437 (1982).

[23]B. Yaakobi, J. Delettrez, L. M. Goldman, R. L. McCrory, W. Seka, and J. M. Soures, Opt. Commun. **41,** 355 (1982).

Downloaded 31 Oct 2003 to 132.170.162.242. Redistribution subject to AIP license or copyright, see http://ojps.aip.org/phf/phfcr.jsp